AIAA JOURNAL
Vol. 31, No. 8, August 1993

Computation of Crossing Shock/Turbulent Boundary Layer Interaction at Mach 8.3

N. Narayanswami*
Rutgers University, Piscataway, New Jersey 08855
C. C. Horstman†
NASA Ames Research Center, Moffett Field, California 94035
and
D. D. Knight‡
Rutgers University, Piscataway, New Jersey 08855

A three-dimensional hypersonic crossing shock wave/turbulent boundary-layer interaction is examined numerically at Mach 8.3. The test geometry consists of a pair of opposing sharp fins of angle $\alpha = 15$ deg mounted on a flat plate. Two theoretical models are evaluated. The full three-dimensional Reynolds-averaged Navier-Stokes equations are solved using the Baldwin-Lomax and the Rodi (modified k-ϵ) turbulence models. Computed results for both cases show good agreement with experiment for flat plate surface pressure and for flowfield profiles of pitot pressure and yaw angle, indicating that the flowfield is primarily rotational and inviscid. Fair to poor agreement is obtained for surface heat transfer, indicating a need for more accurate turbulence models. The overall flowfield structure is similar to that observed in previous crossing shock interaction studies.

I. Introduction

WITH the resurgence of interest in high speed flight in recent years,[1] the problem of viscous-inviscid interaction in aerodynamic flows is once again receiving wide attention. Of particular importance is the phenomenon of three-dimensional shock wave/turbulent boundary-layer interactions ("three-dimensional turbulent interactions"). Such interactions occur in a wide variety of practical aerodynamic situations (e.g., in flows over aircraft control surfaces and within high speed inlets) and are of interest not only due to the inherent complexity and richness of the flow physics but also due to engineering challenges posed by associated problems such as large scale flow separation and increased drag and aerodynamic heating.[1,2]

The present study focuses on the three-dimensional crossing shock interaction (Fig. 1) which is typical of hypersonic inlets. The flow geometry consists of two opposing sharp fins mounted on a flat plate. The oblique shock waves, generated by the fins, intersect each other and interact with the flat plate turbulent boundary layer. Experimental investigations of crossing shock interactions include Mee et al.,[3] Batcho et al.,[4] Williams and Hingst,[5] Garrison and Settles,[6] Garrison et al.,[7] and Kussoy and Horstman.[8] Theoretical (computational) investigations include Gaitonde and Knight,[9] Narayanswami et al.,[10,11] and Reddy.[12] Computations have been performed at Mach 3-8.3 using the three-dimensional Reynolds-averaged Navier-Stokes (RANS) equations incorporating the Baldwin-Lomax turbulence model.[13] The computed flowfields have displayed generally good agreement with experiment for surface pressure and flowfield profiles of pitot pressure and yaw angle. The computed heat transfer has shown substantial error in comparison with experiment. With the exception of a single computation[10] of a crossing shock interaction at Mach 3 using the k-ϵ model,[14] no turbulence model other than the Baldwin-Lomax has been examined for the crossing shock interaction.

The objectives of the present study are as follows.

1) Determine the importance of viscous and inviscid effects in a 3-D hypersonic crossing shock interaction. The flowfields associated with the two individual three-dimensional single fin interactions (upstream of the crossing shock interaction) have been observed to be primarily rotational and inviscid,[15] except

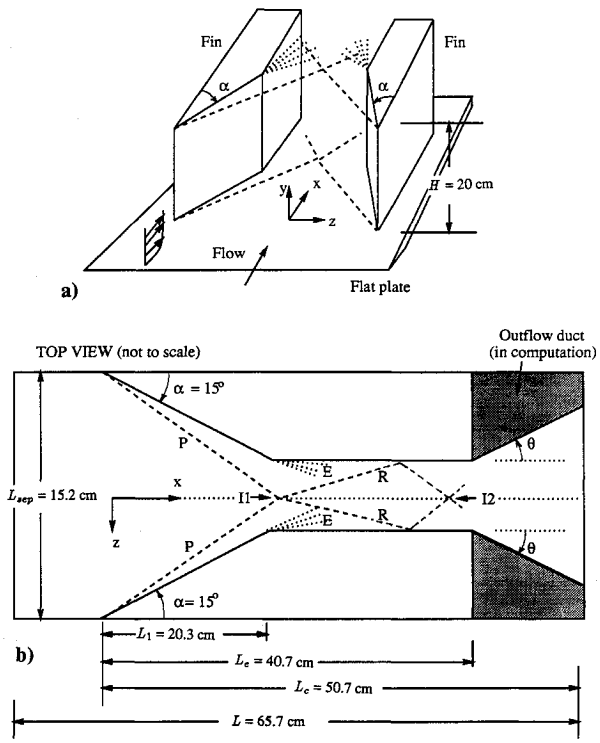

Fig. 1 Crossing shock interaction: a) experimental domain, b) computational domain; α = fin angle, θ = outflow duct angle, P = primary shock, E = expansion fan, R = reflected shock, I1, I2 = location of intersection of primary, reflected shocks, respectively.

Received Aug. 24, 1992; revision received Feb. 1, 1993; accepted for publication Feb. 8, 1993.

*Research Staff, Department of Mechanical and Aerospace Engineering; currently, Shock Wave Research Center, Tohuku University, Sendai, Japan. Member AIAA.

†Senior Scientist, Fluid Dynamics Division. Associate Fellow AIAA.

‡Professor, Department of Mechanical and Aerospace Engineering. Associate Fellow AIAA.

in a thin layer adjacent to the solid surfaces where viscous effects (i.e., turbulent and molecular stresses and heat transfer) are significant. Similar behavior is anticipated for the crossing shock interaction. The present case represents a significant test of this hypothesis since it is the strongest crossing shock interaction studied to date. The overall inviscid pressure rise (≈ 45) is more than twice the previous[11] strongest case (i.e., 19.5).

2) Evaluate the accuracy of the Baldwin-Lomax[13] and Rodi (modified k-ϵ)[16] turbulence models for predicting surface heat transfer. Surface heat transfer is a sensitive test of the accuracy of turbulence models. The accurate prediction of surface heat transfer is critical to the design of inlets for hypersonic vehicles (e.g., the National AeroSpace Plane[1]). Two turbulence models were selected for evaluation. The algebraic Baldwin-Lomax model was chosen for its simplicity (and hence computational efficiency), prior successful application to three-dimensional turbulent interactions, and widespread use in the aerospace industry. The two-equation Rodi (modified k-ϵ) model was selected for its potential greater range of applicability (i.e., the model does not require the prescription of a length scale) and its close similarity to the k-ϵ model which has become more commomly used by the aerospace industry. The Rodi modification to the k-ϵ model is employed since the k-ϵ model in its original form cannot self-generate a turbulent boundary layer from the leading edge of a plate. Further, the Rodi model has been found to yield better results than the original k-ϵ model for two-dimensional separated flows.[16]

In previous studies of the three-dimensional single fin interaction, both algebraic and two-equation turbulence models have predicted the surface heat transfer with reasonable accuracy in comparison with experiment. At Mach 5.0, Rodi et al.[17] obtained agreement within 33% at $\alpha = 8$ and 16 deg using the Baldwin-Lomax model. At Mach 5.9, Hung and MacCormack[18] obtained agreement within 15% at $\alpha = 6$ deg and within 28% at $\alpha = 12$ deg using the algebraic Escudier model. However, with increasing shock strength, the level of accuracy has decreased. At Mach 8.3, Knight et al.[19] obtained agreement within 36% at $\alpha = 10$ deg and within 48% at $\alpha = 15$ deg using both the k-ϵ and Rodi models.

The present case, however, represents a more stringent test of the capability of the turbulence models to predict surface heat transfer. The overall inviscid pressure ratio (≈ 45) is substantially greater than any three-dimensional single fin interaction studied. Additionally, the flowfield structure is more complicated due to the interacting shock structures.

3) Determine the flowfield structure of the crossing shock interaction. This objective relies on the successful validation of the theoretical model(s). The flowfield structure is determined through analysis of the computed results and compared with previous studies for supersonic crossing shock interactions.

II. Description of Experiment

The experiments were conducted in the 3.5-ft hypersonic wind tunnel at the NASA Ames Research Center.[8] The freestream conditions are shown in Table 1. The incoming boundary layer was fully developed and self-preserving at the fin leading-edge location with a velocity profile matching the law of wall and wake.[20] The experimental geometry is shown in Fig. 1. The fin height $H = 20$ cm ($6.2\delta_\infty$) was sufficient to ensure a semi-infinite interaction. Disturbances generated by the top edges of the fins had no effect on the interaction in the region of interest, as confirmed a posteriori by the fin surface flow visualization results. The total fin length is $L_e = 40.7$ cm ($12.5\delta_\infty$). At a streamwise location of $L_1 = 20.3$ cm ($6.2\delta_\infty$), the fin surfaces are turned parallel to the streamwise (x) direction. The separation distance between the fin leading edges is $L_{sep} = 15.2$ cm ($4.7\delta_\infty$).

III. Description of Computations

The flow conditions closely match the experiment (refer to Table 1). Only approximate values of the flow conditions were known at the time of the computation, resulting in minor discrepancies between the theoretical and actual experimental values of Mach number M_∞ and total pressure $P_{t\infty}$ (and, consequently, in the boundary-layer thickness parameters and Reynolds number Re_{δ_∞}).

The governing equations are the three-dimensional Reynolds-averaged Navier-Stokes equations using mass averaged variables in strong conservation form.[21] The Baldwin-Lomax and the Rodi (modified k-ϵ) turbulence models were employed. The molecular dynamic viscosity was specified by Sutherland's law. The molecular Prandtl number is 0.73 (air) and the turbulent Prandtl number is 0.9. The perfect gas equation of state was employed, since real gas effects are negligible under the present flow conditions.[22]

For simplicity, the fin boundary layer was assumed to be turbulent from the leading edge. In the experiment, the fin boundary layer (in the region outside of the plate boundary layer) transitions to turbulent at approximately 21 cm downstream of the fin leading edge (based on the method of Ref. 23). However, the flowfield in the region of interest is unaffected by the location of transition on the fins as indicated in previous computations by Knight et al.[19] for the three-dimensional single fin interaction at Mach 8.2 and by Narayanswami et al.[11] for the $\alpha = 10$-deg crossing shock interaction at Mach 8.3.

Flow symmetry permitted computation of one-half of the flow domain. On the inflow boundary, the two-dimensional turbulent boundary-layer profile matching the experiment was prescribed. On the plate and fin surfaces, the velocity vector, k, ϵ, and the normal gradient of static pressure were set to zero. The temperature was set to the experimental value. On the symmetry boundaries (upstream of the fin leading edge and the centerplane), the normal component of velocity and the normal derivatives of the remaining velocity components, static pressure, temperature, and k and ϵ were set to zero. A zero gradient condition was employed at the top and outflow boundaries. The Baldwin-Lomax and Rodi computations employed the hybrid schemes of Knight[24] and MacCormack,[25] respectively.

In the experiment (Fig. 1b), the fins are terminated at a distance $L_e = 40.7$ cm. In the computations, a diverging duct of angle θ is added to simplify grid generation where $\theta = 20$ and 10 deg for the Baldwin-Lomax and Rodi computations, respectively. The streamwise length of the computational domain was extended to $L_c = 50.7$ and 55.55 cm for the Baldwin-Lomax and Rodi cases, respectively. The inclusion of the duct does not affect the flowfield in the region surrounding the crossing shocks, since the computed flowfields at $x = L_e$ were supersonic everywhere except extremely close to the plate and fin surfaces.

The grids adequately resolve the flowfield and meet all the criteria for grid resolution employed in previous three-dimensional turbulent interaction studies.[7,10,11,15] The grid spacing for the Baldwin-Lomax computation is the same as that employed in the Mach 8.3, $\alpha = 10$-deg crossing shock interaction study[11] wherein a grid refinement study was performed. Details of the grids are provided in Table 2. The total number of grid points and degree of resolution in the two computations are similar. The inflow boundary is in a region of undisturbed flow. Nonuniform spacing is employed in all three directions. The minimum x grid spacing ($0.15\delta_\infty$) is in the region sur-

Table 1 Flow conditions[a]

	δ_∞, cm	δ^*_∞, cm	M_∞	Re_{δ_∞}	$P_{t\infty}$, kPa	$T_{t\infty}$, K	T_w, K
Experiment	3.25	1.26	8.28	1.7×10^5	5220	1111	300
Baldwin-Lomax	3.0	1.38	8.20	1.6×10^5	4900	1111	300
Rodi	3.0	1.22	8.18	1.6×10^5	4822	1111	300

[a]Legend: δ = boundary layer thickness, δ^* = displacement thickness, M = Mach number, Re = Reynolds number, P_t = total pressure, T_t = total temperature, T_w = wall temperature (fin and plate surfaces); subscripts: ∞ = evaluated in freestream, δ = evaluated based on boundary-layer thickness.

Table 2 Grid details[a]

	N_x	$\Delta x/\delta_\infty^\dagger$	x_{inflow}/δ_∞	$x_{outflow}/\delta_\infty$
		x Direction		
Baldwin-Lomax	100	0.15	−4.63	15.6
Rodi	100	0.15	−1.26	17.1
	N_y	$\Delta y/\delta_\infty\|_{min}$	$\Delta y/\delta_\infty\|_{max}$	y_{max}/δ_∞
		y Direction		
Baldwin-Lomax	72	0.56×10^{-4}	0.16	7.39
Rodi	64	0.25×10^{-4}	0.14	6.0
	N_z	$\Delta z/\delta_\infty\|_{min}$	$\Delta z/\delta_\infty\|_{max}$	z_{max}/δ_∞
		z Direction		
Baldwin-Lomax	35	1.81×10^{-4}	0.22	2.34
Rodi	40	0.25×10^{-4}	0.1	2.34

	$\Delta y^+\|_{plate}$			$\Delta z^+\|_{fin}$		
	avg	max	N_{plate}	avg	max	N_{fin}
Baldwin-Lomax	0.18	0.63	30	0.67	1.97	20
Rodi	0.4	1.0	30	0.3	1.0	20

[a]Legend: δ = boundary layer thickness; N_x, N_y, N_z = number of points along *x*, *y*, and *z* directions, respectively; Δx, Δy, Δz = grid spacings in the *x*, *y*, and *z* directions, respectively; $\Delta y^+|_{plate}$, $\Delta z^+|_{fin}$ = distance of first point adjacent to flat plate and fin surfaces, respectively; N_{plate}, N_{fin} = typical number of points in the boundary layer on flat plate fin surfaces, respectively; subscripts: in, out = at inflow, outflow planes; max = maximum; min = minimum; ∞ = evaluated in freestream; superscripts: † implies variable grid spacing; reported values are in vicinity of inviscid shock intersection; + implies wall units, i.e., distances are normalized by the local viscous length scale ν_w/u_*.

rounding the crossing shocks. In the crossflow (*y*-*z*) plane, simple geometrically stretched grids are employed with minimum spacings adjacent to the solid surfaces. In the Baldwin-Lomax computation, the first point adjacent to the plate satisfies $y^+ \leq 0.63$ at all locations, where $y^+ = yu^*/\nu_w$ and $u^* = \sqrt{\tau_w/\rho_w}$ is the local friction velocity, τ_w the wall shear stress, ρ_w the density at the wall, and ν_w the kinematic viscosity at the wall. The average value of y^+ is 0.18. The first point off the fin surface satisfies $z^+ \leq 2.0$, the average value being 0.67. In the Rodi computation, the first point off the flat plate and fin surfaces satisfies $y^+ \leq 1.0$ and $z^+ \leq 1.0$, the average values being 0.4 and 0.3, respectively. The plate and fin boundary layers contain typically 30 and 20 grid points, respectively, in both computations. The maximum spacing in the *y* direction (in the freestream) is $0.16\delta_\infty$ for the Baldwin-Lomax case and $0.14\delta_\infty$ for the Rodi case. The spacing in the *z* direction in the freestream varies along the streamwise (*x*) direction, due to narrowing of the physical domain. The maximum *z*-grid spacing is $0.22\delta_\infty$ for the Baldwin-Lomax computation and $0.1\delta_\infty$ for the Rodi computation, at the upstream boundary.

The initial condition in both computations was obtained by propagating the two-dimensional inflow boundary-layer profile to all downstream locations. Convergence was determined by monitoring changes in specific flow variables (density, streamwise velocity, and total energy) over characteristic time spans T_c ($= L/U_\infty$). At convergence, the relative change in the given flow variables over $1T_c$ was typically less than 0.1% at all locations. Further, the relative change of all the flow variables with respect to freestream conditions was less than 0.1% at all locations at convergence. The computations each required a total integration time of approximately 4–5 T_c for convergence.

IV. Comparison with Experiment

In all of the results to be presented (Figs. 3–12), the dimensions *x*, *y*, and *z* have been normalized by the experimental upstream boundary-layer thickness $\delta_\infty = 3.25$ cm. The experimental uncertainty levels shown are fixed percentages of the absolute values. The estimated uncertainties in the various measured quantities are the larger of ± 10% and ± 80 N/m^2 for static pressure, ± 5% for pitot pressure, ± 3 deg for yaw angle, ± 10% for surface heat transfer, and ± 0.02 cm in the *y* coordinate (normal to the flat plate). The uncertainties were determined from run-to-run measurement scatter, comparison of different measurement techniques, and instrument accuracy. The corresponding computational uncertainties (based on a grid resolution study reported in Ref. 11) is ± 5% for all of the given flow quantities for the Baldwin-Lomax case. The uncertainty in the Rodi computation is comparable.

A. Surface Pressure

Comparison between the computed and experimental surface pressure distribution shows good agreement. Experimental flat plate surface pressure measurements were taken along the interaction centerline and along transverse cuts at various streamwise locations (Refer to Fig. 2). Along the centerline (Fig. 3), the general shape of the distribution, extent of upstream influence, and the locations of the first maximum (at $x/\delta_\infty = 6.8$) and minimum (at $x/\delta_\infty = 9.0$) are predicted reasonably well by both computations. The peaking of the pressure is a result of the intersection of the primary shocks (see "I1" in Fig. 1b). The subsequent drop in pressure results from the expansion fan originating at the turn in the fin geometry at $x/\delta_\infty = 6.26$ (see "E" in Fig. 1b). The magnitude of the peak pressure is overpredicted in both cases by approximately 20%. The observed peak pressure is nearly one-half of the inviscid value, indicating significant combined influence of viscous effects and the expansion fan. A second (smaller) peak is observed farther downstream at approximately $x/\delta_\infty = 10.0$ and is associated with the second crossing of the reflected shocks (see "I2" in Fig. 1b). The magnitude of this second peak and the general distribution of pressure downstream of $x/\delta_\infty = 9.5$ are predicted accurately by the Baldwin-Lomax computation but are overestimated in the Rodi case. Examination of the experimental fin surface streamlines (not shown)

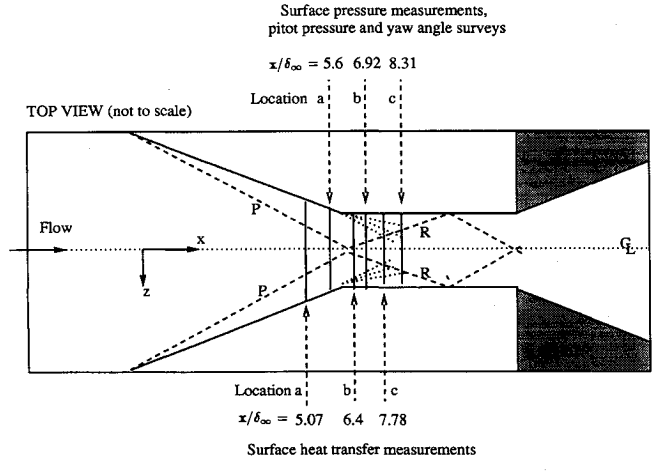

Fig. 2 Location of experimental measurements.

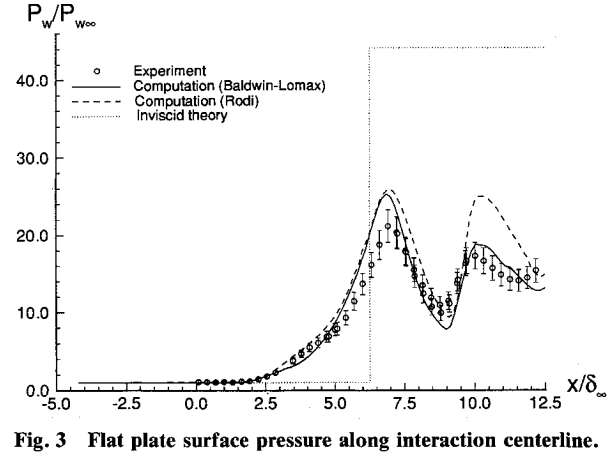

Fig. 3 Flat plate surface pressure along interaction centerline.

indicates significant streamwise separation at approximately $x/\delta_\infty = 6.5$. Similar results are observed for the Baldwin-Lomax computation. The Rodi computation, however, does not show any such streamwise separation. Consequently, in the Rodi case, the shocks reflecting off the fin surfaces are stronger than in the Baldwin-Lomax case and lead to higher pressures downstream of their intersection. Along the transverse cuts at $x/\delta_\infty = 5.6$, 6.92, and 8.31 (refer to Fig. 2), the computed results show similar good agreement with experiment (Fig. 4). A discussion of the flow physics associated with the profile shape and magnitude of pressure along each transverse cut is provided in Ref. 26.

B. Pitot Pressure

The experimental and computed results for pitot pressure ($P_p/P_{p\infty}$) are shown in Figs. 5a–5f. The results are displayed as color contours on crossflow (y–z) planes (locations shown in Fig. 2). Note that a separate color scale is used for each plane. Locations (Figs. 5a, 5b), (Figs. 5c, 5d), and (Figs. 5e, 5f) correspond to $x/\delta_\infty = 5.6$, 6.92, and 8.31, respectively. The experimental measurements do not extend fully to the fin and plate surfaces. The region of computation is truncated to match the region of experimental measurement.

There is overall good agreement between the experiment and both computations. At $x/\delta_\infty = 5.6$ (Figs. 5a, 5b), a large low pitot pressure region (marked "1") is observed in the region $y/\delta_\infty < 0.8$. This structure[10,11] is associated with a low total pressure jet comprising two helical counter-rotating vortices (see Sec. V.A), and is evident at subsequent stations (Figs. 5c–5f). The sharp change of contour levels in the region $0.1 \le z/\delta_\infty \le 0.2$, $y/\delta_\infty > 1.0$ indicates the primary shock. The shape and extent of the low pitot pressure region are predicted fairly accurately by both computations. At $x/\delta_\infty = 6.92$ and 8.31 (Figs. 5c–5f), there is general qualitative agreement between the computations and experiment, with the Rodi computation displaying overall better accuracy than the Baldwin-Lomax computation. In both cases, the computed low pitot pressure region is somewhat flattened, compared to the experiment.

C. Yaw Angle

The computed and experimental results for yaw angle profiles in the flowfield show overall general agreement (Figs. 6–8). The yaw angle is defined by $\tan^{-1}(w/u)$ where w and u are the velocities in the z (crossflow) and x (streamwise) directions, respectively, and represents the local direction of the velocity vector in a plane parallel to the flat plate. The experimental surveys were taken at $x/\delta_\infty = 5.6$, 6.92, and 8.31 (refer to Fig. 2). At $x/\delta_\infty = 5.6$ (Fig. 6), the locations a–d denote distances *away* from the centerline of $z/\delta_\infty = -0.65$, -0.49, -0.33, and -0.16, respectively (i.e., the survey stations are to the left of the centerline). At locations $x/\delta_\infty = 6.92$ (Fig. 7) and $x/\delta_\infty = 8.31$ (Fig. 8), the locations a–c represent $z/\delta_\infty = -0.48$, -0.32, and -0.15, respectively. The particulars of the flow physics associated with each of the profiles is discussed in detail in Ref. 26.

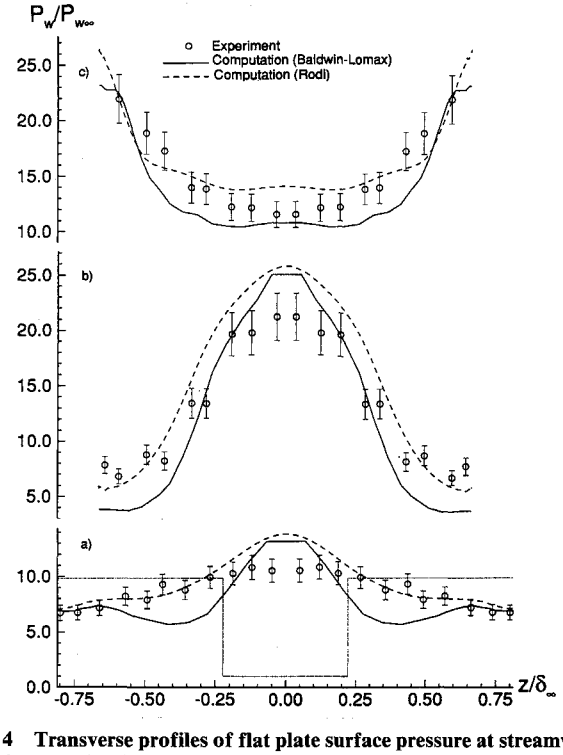

Fig. 4 Transverse profiles of flat plate surface pressure at streamwise locations of a) $x/\delta_\infty = 5.6$, b) $x/\delta_\infty = 6.92$, and c) $x/\delta_\infty = 8.31$.

At each of the experimental survey stations, the yaw angles are in general larger in magnitude than the local pitch angle values. The maximum pitch angles at locations a–d (determined for the Baldwin-Lomax computation) for $x/\delta_\infty = 5.6$ are -8.5, -8.5, -4.5, and 14.0 deg, respectively. For $x/\delta_\infty = 6.92$, the maximum pitch angles for locations a–c are -8.5, -10, and 4.0 deg, respectively. The corresponding values for $x/\delta_\infty = 8.31$ are -8.5, -7.5, and -5.0 deg, respectively.

In summary, the comparison of computed and experimental surface pressure, pitot pressure, and yaw angle yield two important results. First, the calculations using both the Baldwin-Lomax and Rodi models are in general agreement with experiment. Second, the two models are in close agreement with each other. However, the computed turbulent eddy viscosity profiles[26] exhibit differences as large as a factor of seven within the boundary layer. This observation, coupled with the previous two results, confirms the hypothesis (Sec. I) that the flowfield is principally rotational and inviscid, except in a thin layer adjacent to the solid surfaces where viscous effects (i.e., turbulent and molecular stresses and heat transfer) are significant.

D. Surface Heat Transfer

As discussed in Sec. I, the accurate prediction of surface heat transfer represents a critical test of the accuracy of turbulence models. Experimental flat plate heat transfer measurements were taken along the interaction centerline and along transverse cuts at the streamwise locations of $x/\delta_\infty = 5.07$, 6.4, and 7.78 (refer to Fig. 2). The measurements were taken using both thermocouples and Schmidt-Boelter gauges.[8]

The computed and experimental surface heat transfer distributions show overall fair to poor agreement. The computed and experimental results along the centerline are shown in Fig. 9. Both computations show good qualitative agreement with experiment with regard to the general shape of the profile. The initial drop in heat transfer in the region $1.0 \le x/\delta_\infty \le 3.0$ is predicted more accurately by the Baldwin-Lomax computation. However, there is significant disagreement between both computations and experiment in the region $3.0 \le x/\delta_\infty \le 5.0$; the Baldwin-Lomax computation underestimates the heat transfer by as much as 90%. Beyond $x/\delta_\infty = 5.0$, the Baldwin-Lomax computation shows better overall agreement with the experimental data than the Rodi computation. The peak heat transfer is overpredicted by both computations by approximately 20%.

The comparison between computation and experiment along transverse cuts (Figs. 10a–10c) shows poor agreement. Both computations generally overpredict the experimental values. At $x/\delta_\infty = 6.4$ and 7.78 (locations b and c), the peak heat transfer is overestimated by the Baldwin-Lomax computation by as much as 50% and 85%, respectively. The overestimation in the Rodi case is comparable. The sharply peaked distributions in the case of the Baldwin-Lomax computation is due to sharp changes in the magnitude of the local length scale computed by the turbulence model.

The significant disagreement between computed and experimental surface heat transfer implies an inadequate modeling of the turbulence (at least, near the wall) by both models. Despite its greater potential range of applicability, the two-equation Rodi model overall shows no significant improvement compared to the algebraic Baldwin-Lomax model. Per-

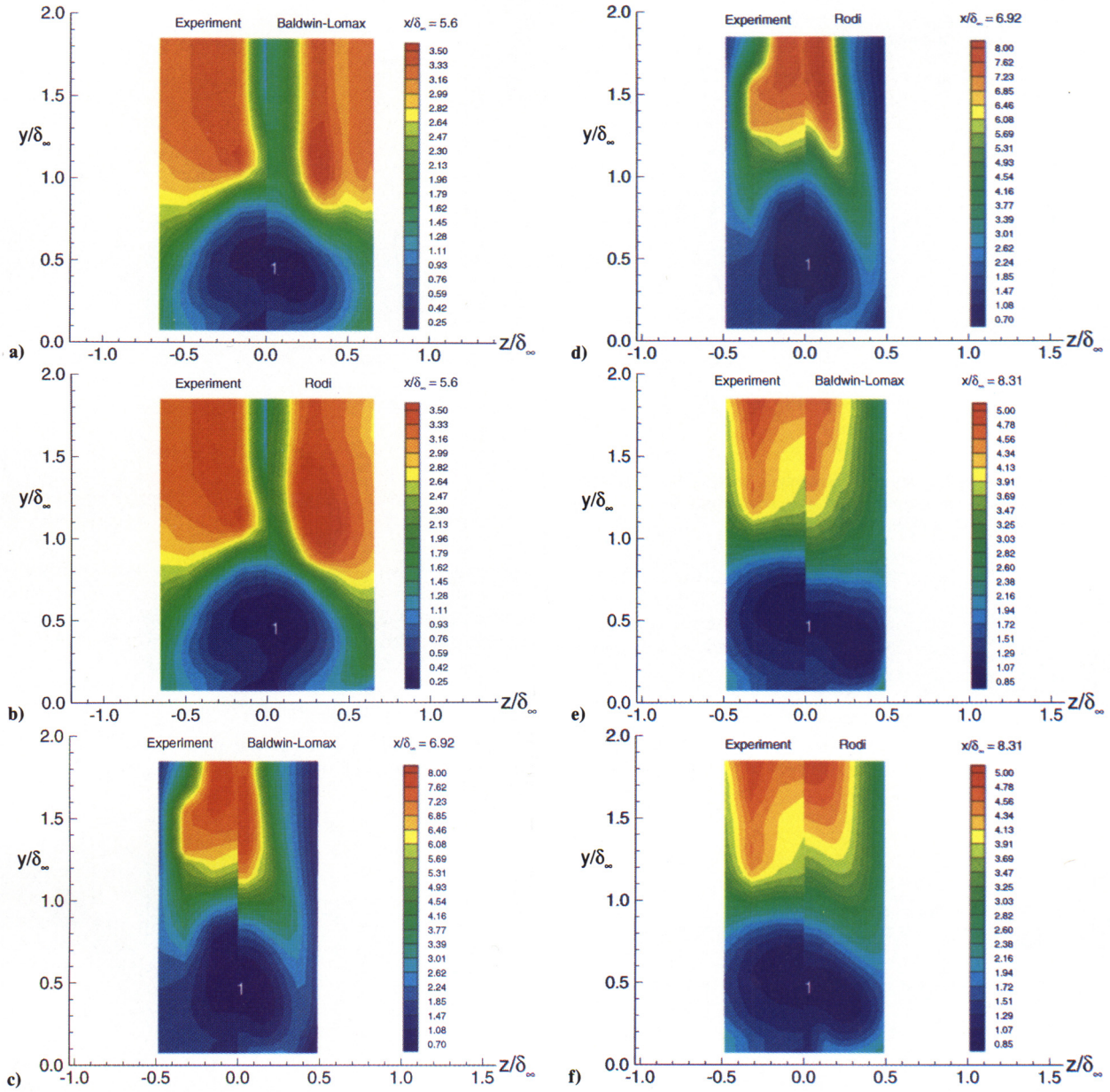

Fig. 5 Experimental and computed pitot pressure contours on crossflow planes at a) and b) $x/\delta_\infty = 5.6$, c) and d) $x/\delta_\infty = 6.92$, and e) and f) $x/\delta_\infty = 8.31$; and 1 = low pitot pressure jet.

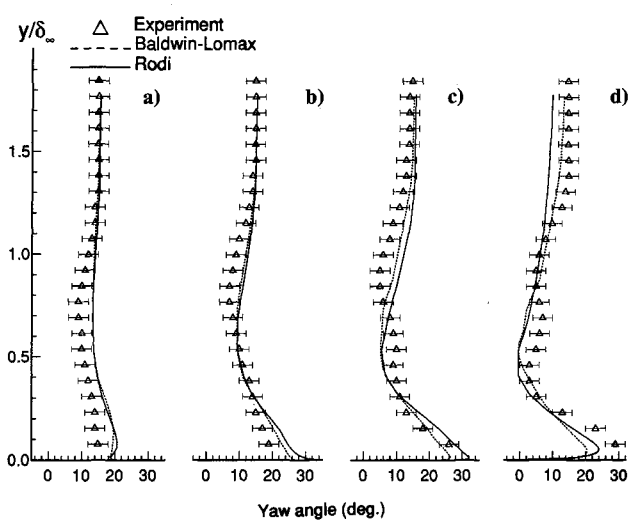

Fig. 6 Experimental and computed yaw angle profiles (in deg) at $x/\delta_\infty = 5.6$: locations measured from the centerline, a) $z/\delta_\infty = -0.65$, b) $z/\delta_\infty = -0.49$, c) $z/\delta_\infty = -0.33$, and d) $z/\delta_\infty = -0.16$.

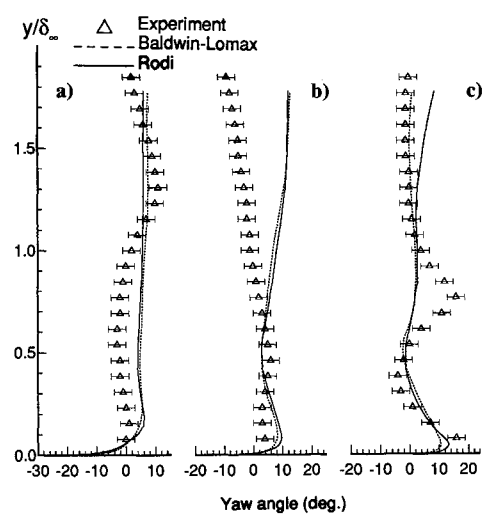

Fig. 7 Experimental and computed yaw angle profiles (in deg) at $x/\delta_\infty = 6.92$: locations measured from the centerline, a) $z/\delta_\infty = -0.48$, b) $z/\delta_\infty = -0.32$, and c) $z/\delta_\infty = -0.15$.

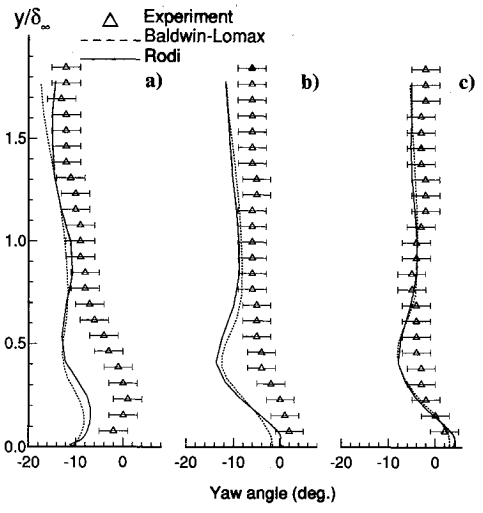

Fig. 8 Experimental and computed yaw angle profiles (in deg) at $x/\delta_\infty = 8.31$: locations measured from the centerline, a) $z/\delta_\infty = -0.48$, b) $z/\delta_\infty = -0.32$, and c) $z/\delta_\infty = -0.15$.

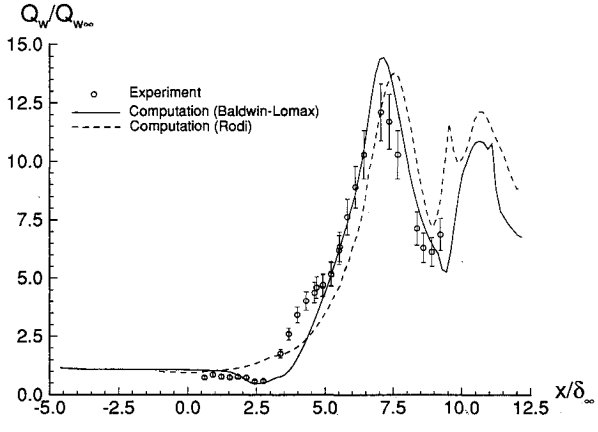

Fig. 9 Flat plate surface heat transfer along interaction centerline.

haps the assumption of a turbulent eddy viscosity, common to both models, is responsible for the discrepancies between prediction and experiment. Clearly, further research in compressible turbulence modeling is needed, including perhaps Reynolds stress equation models.

V. Flowfield Structure

Notwithstanding the discrepancy between the computed and experimental values of surface heat transfer, the prediction of the flowfield (at least away from the solid surfaces) is fairly accurate in both computations, as evidenced by the overall good agreement between the computations and experiment for surface pressure and pitot pressure and yaw angle profiles. The computed results are thus analyzed to determine the flowfield structure of the interaction.

A. Streamline Structure

The streamline structure of the interaction determined from both the Baldwin-Lomax and Rodi computations show close agreement. The structure is similar to that observed in previous studies of crossing shock interactions.[7,10,11] The principal feature of the streamline structure is a low total pressure jet comprising two weakly counter-rotating vortices whose cores are formed by streamlines originating close to the flat plate within the incoming boundary layer. The computed trajectories of particles originating at $y/\delta_\infty = 0.25$ (Fig. 11a) clearly show the two vortices that are initially formed by the individual single fin interactions[15] in the upstream portion of the

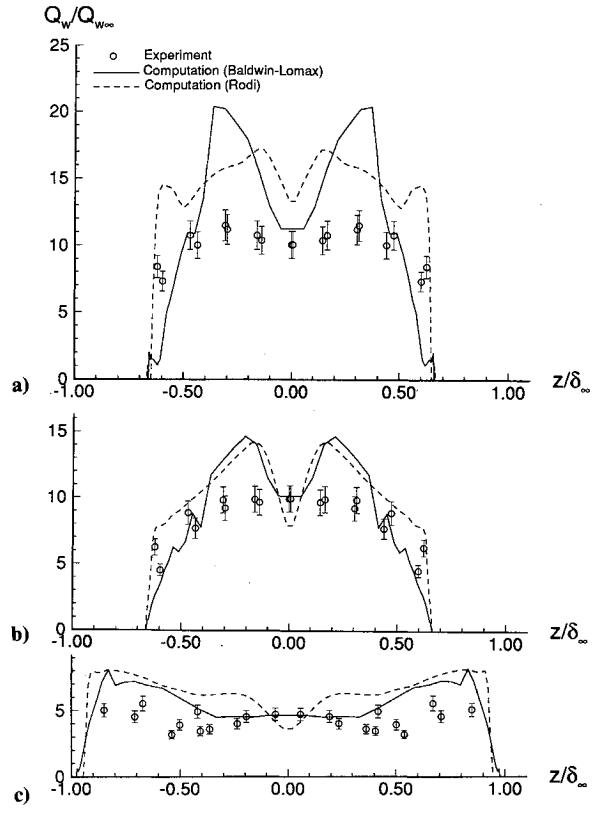

Fig. 10 Transverse profiles of flat plate surface heat transfer at streamwise locations of a) $x/\delta_\infty = 5.07$, b) $x/\delta_\infty = 6.4$, and c) $x/\delta_\infty = 7.78$.

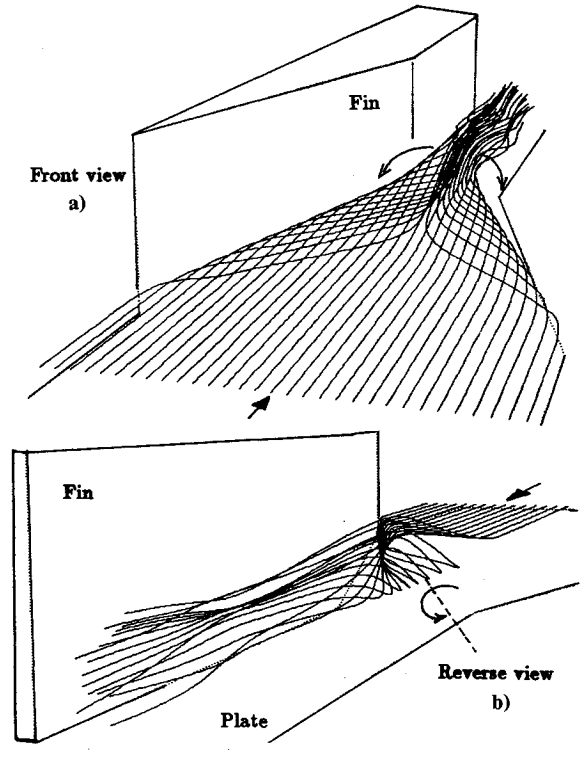

Fig. 11 Vortical structures formed by streamlines originating at a level of $y/\delta_\infty = 0.25$ in the upstream boundary layer (Baldwin-Lomax computation); a) front perspective view and b) reverse perspective view (only one of the vortices is shown).

flow. One of the vortices is shown in the reverse perspective view in Fig. 11b. The two vortices "collide" at the centerline and are lifted away from the flat plate in the form of a jet. This jet structure is also evident from the low pitot pressure contours observed in Figs. 5a–5f. Two smaller counter-rotat-

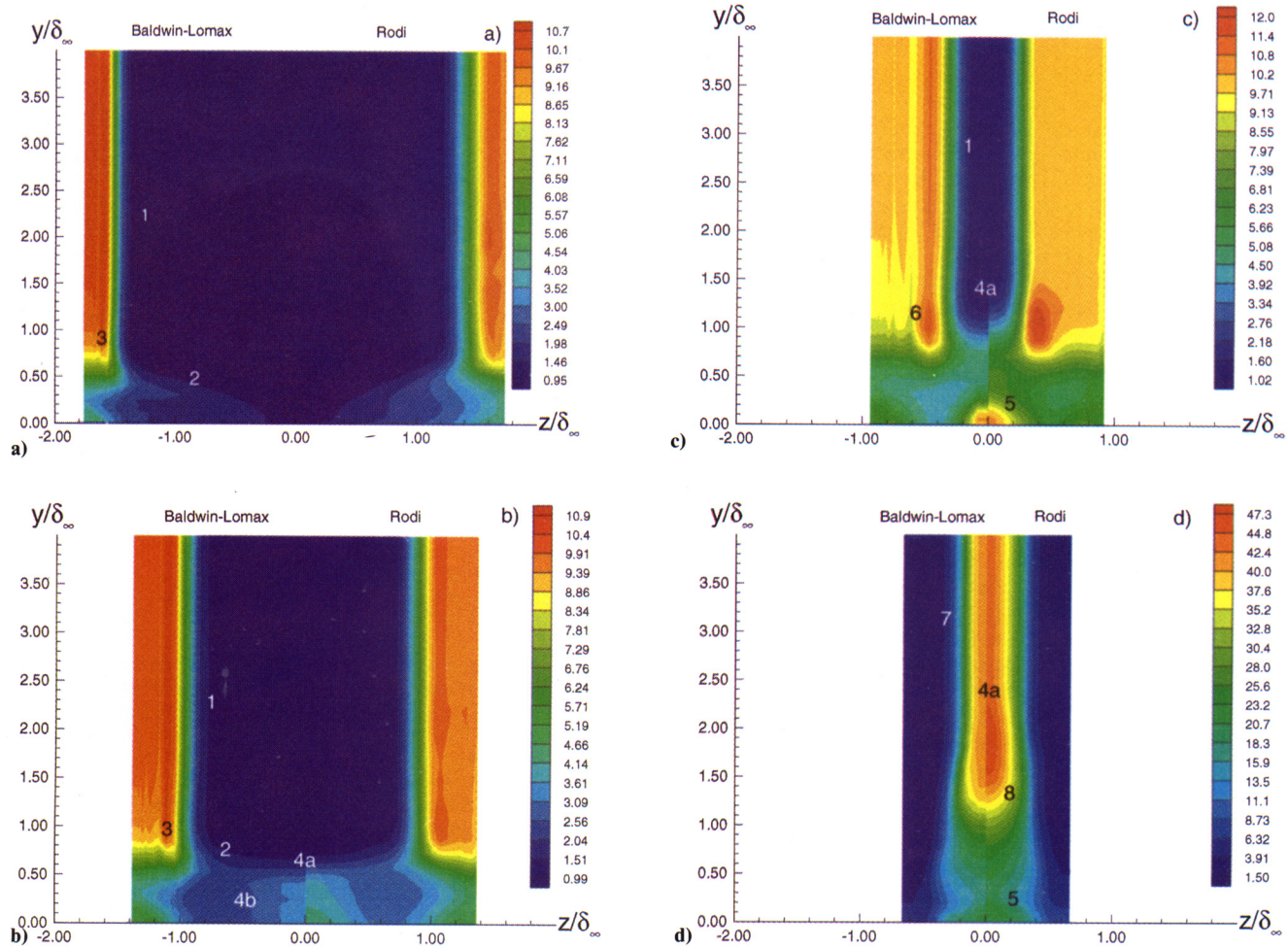

Fig. 12 Computed static pressure contours on crossflow planes at a) $x/\delta_\infty = 2.15$, b) $x/\delta_\infty = 3.57$, c) $x/\delta_\infty = 5.23$, and d) $x/\delta_\infty = 7.38$; 1 = primary shock, 2 = separation shock, 3 = rear shock, 4a = central segment of conical shock, 4b = curved segment of conical shock, 5 = centerline shock, 6 = high-pressure region, 7 = reflected shock, and 8 = expansion.

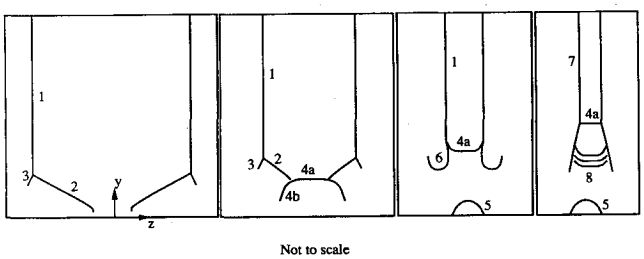

Fig. 12e Schematic of flowfield wave structure: 1 = primary shock, 2 = separation shock, 3 = rear shock, 4a = central segment of conical shock, 4b = curved segment of conical shock, 5 = centerline shock, 6 = high-pressure region, 7 = reflected shock, and 8 = expansion.

ing vortices (not shown here) are present close to the fin-plate junctions, beneath the two large vortices forming the jet. Streamlines originating from near the edge of the incoming boundary layer (e.g., $y/\delta_\infty = 0.75$, not shown) wrap around and underneath the lifting low total pressure jet (note the relatively higher pitot pressures away from the centerline at the base of the low pitot pressure regions in Figs. 5a–5f). Streamlines originating from above $y/\delta_\infty = 1.0$ in the upstream boundary layer are deflected by the local "inviscid" portions of the primary and reflected shocks and continue streamwise over the low total pressure jet underneath.

B. Wave Structure

The wave structure of the interaction is generally similar to previous observations of crossing shock interactions[7,10] at supersonic Mach numbers. Figs. 12a–12d show contours of static pressure (P/P_∞) on crossflow (y-z) planes at $x/\delta_\infty = 2.15$, 3.57, 5.23, and 7.38, respectively. The color bar indicates the range of P/P_∞ on the particular crossflow plane. A schematic of the shock waves and expansion fans determined from the static pressure contours at each location is shown in Fig. 12e.

The two computations show close agreement. The comparison is shown by presenting the results of the two cases as the two halves of the crossflow plane. At location Fig. 12a, ($x/\delta_\infty = 2.15$), the λ-shaped shock structures of the individual single fin interactions are evident. The primary shock (1) bifurcates[27] into a separation shock (2) and a rear shock (3). A slip line (not shown) emanates from the triple point (intersection of shocks 1, 2, and 3) and curves into the fin-plate junction. The separation vortex is aligned approximately with the primary shock, at the base of the shock. The flow between the vortex and slip line is turned by an expansion fan (not shown). At location Fig. 12b ($x/\delta_\infty = 3.57$), a conical ∩-shaped reflected shock (4a, 4b) has developed due to the interaction of the two separation shocks. This conical shock grows outward, away from the centerline. At location Fig. 12c ($x/\delta_\infty = 5.23$), the interaction of the curved portion of the conical shock (4b) with the rear shock (3) has resulted in a region of local high pressure (6). The central segment of the conical shock (4a) remains unaffected. A new shock structure (5) is formed over the flat plate near the interaction centerline. At location Fig. 12d ($x/\delta_\infty = 7.38$), the primary shocks have crossed. The reflected shocks (7) are clearly observed. Shock 4a appears to continue upward, between the reflected shocks. An expansion fan (8) is formed between the reflected shocks, below shock 4a. The shock over the centerline (5) is still present.

However, there are some differences between the wave structure just discussed and that observed experimentally[6] at Mach 4. In the present case, only the central portion (4a) of the conical shock remains after interaction with the rear shock (3). However, the Mach 4 experimental results indicate that the entire conical shock (including the curved portion 4b) continues to grow outward after interaction with the rear shock. This difference is perhaps due to the fact that the expansion fans originating from the fin surface at $x/\delta_\infty = 6.26$ in the present case interact with and significantly weaken the curved portions of the conical shock. No such expansion fans were present in the Mach 4 case. There is a clear need for direct experimental flowfield visualization of the present case to resolve these issues.

VI. Conclusions

The three-dimensional crossing shock interaction at Mach 8.3 for symmetric 15-deg fins was investigated theoretically (numerically) using the Reynolds-averaged Navier-Stokes equations and two turbulence models. The following conclusions have been reached.

1) The flowfield is primarily rotational and inviscid, except in a thin layer adjacent to solid surfaces where viscous effects (i.e., turbulent and molecular stresses and heat transfer) are significant. This conclusion is similar to the result for the three-dimensional single fin and is based on the close agreement between the computational results for surface pressure and profiles of pitot pressure and yaw angle, despite considerable differences in the computed eddy viscosity distributions.

2) Neither turbulence model accurately predicts surface heat transfer. The peak heat transfer off centerline is overestimated by as much as 85%. This error is approximately twice the maximum error observed for heat transfer predictions in three-dimensional single fin studies. Further research is needed to develop more accurate turbulence models.

3) The streamline and wave structure is similar to the results at lower (supersonic) Mach numbers. The principal feature of the streamline structure is the formation of a low total pressure jet comprising two weakly counter-rotating vortices. The wave structure involves complex shock wave and expansion fan systems. The flowfield structure predicted by both turbulence models are in close agreement.

Acknowledgments

This research was sponsored by the AFOSR under Grant 86-0266 monitored by L. Sakell. Supercomputer resources were provided by the National Center for Supercomputing Applications (NCSA) by Cray Research Inc. through the University Research and Development Grant program and by the NASA Ames Research Center. Analysis of the computed results was performed at the Rutgers University-Supercomputer Remote Access Facility.

References

[1]VanWie, D., White, M., and Corpening, G., "NASP Inlet Design and Testing Issues," *Johns Hopkins APL Technical Digest,* Vol. 11, Nos. 3 and 4, 1990, pp. 353–361.

[2]Settles, G., and Dolling, D., "Swept Shock/Boundary Layer Interactions—Tutorial and Update," AIAA Paper 90-0375, Jan. 1990.

[3]Mee, D., Stalker, R., and Stollery, J., "Glancing Interactions Between Single and Intersecting Oblique Shock Waves and a Turbulent Boundary Layer," *Journal of Fluid Mechanics,* Vol. 170, Sept. 1986, pp. 411–433.

[4]Batcho, P., Ketchum, A., Bogdonoff, S., and Fernando, M., "Preliminary Investigation of the Interactions Caused by Crossing Shock Waves and a Turbulent Boundary Layer," AIAA Paper 89-0359, Jan. 1989.

[5]Williams, K. E., and Hingst, W. R., "The Effect of Varying Mach Number on Crossing, Glancing Shocks/Turbulent Boundary Layer Interactions," AIAA Paper 91-2157, June 1991.

[6]Garrison T. J., and Settles, G. S., "Flowfield Visualization of Crossing Shock-Wave/Boundary Layer Interactions," AIAA Paper 92-0750, Jan. 1992.

[7]Garrison, T. J., Settles, G. S., Narayanswami, N., and Knight, D., "Structure of Crossing Shock Wave/Turbulent Boundary Layer Interactions," AIAA Paper 92-3670, July 1992.

[8]Kussoy, M. I., and Horstman, K. C., "Intersecting Shock-Wave/Turbulent Boundary Layer Interactions at Mach 8.3," NASA TM 103909, Feb. 1992.

[9]Gaitonde, D., and Knight, D., "Numerical Experiments on the 3-D Shock Wave-Boundary Layer Interaction Generated by a Sharp Fin," AIAA Paper 88-0309, Jan. 1988.

[10]Narayanswami, N., Knight, D., Bogdonoff, S., and Horstman C., "The Interaction Between Crossing Oblique Shocks and a Turbulent Boundary Layer," *AIAA Journal,* Vol. 30, No. 8, 1992, pp. 1945–1952.

[11]Narayanswami, N., Knight, D., and Horstman, C., "Investigation of a Hypersonic Shock Wave/Turbulent Boundary Layer Interaction," *Shock Waves* (to be published).

[12]Reddy, D. R., "3-D Navier-Stokes Analysis of Crossing, Glancing Shocks/Turbulent Boundary Layer Interactions," AIAA Paper 91-1758, June 1991.

[13]Baldwin, B., and Lomax, H., "Thin Layer Approximation and Algebraic Model for Separated Turbulent Flows," AIAA Paper 78-257, Jan. 1978.

[14]Jones, W., and Launder, B., "The Prediction of Laminarization with a Two-Equation Model of Turbulence," *International Journal of Heat and Mass Transfer,* Vol. 15, 1972, pp. 301–304.

[15]Knight, D., Horstman, C. C., Shapey, B., and Bogdonoff, S., "Structure of Supersonic Turbulent Flow Past a Sharp Fin," *AIAA Journal,* Vol. 25, No. 10, 1987, pp. 1331–1337.

[16]Rodi, W., "Experience with Two-Layer Models Combining the k-ϵ with a One-Equation Model Near the Wall," AIAA Paper 91-0216, Jan. 1991.

[17]Rodi, P. E., Dolling, D. S., and Knight, D. D., "An Experimental/Computational Study of Heat Transfer in Sharp Fin Induced Turbulent Interactions at Mach 5," AIAA Paper 91-1764, June 1991.

[18]Hung, C. M., and MacCormack, R. W., "Numerical Solution of Three-Dimensional Shock Wave and Turbulent Boundary Layer Interaction," *AIAA Journal,* Vol. 16, No. 10, 1978, pp. 1090–1096.

[19]Knight, D. D., Horstman, C. C., and Monson, D. J., "The Hypersonic Shock Wave-Turbulent Boundary Layer Interaction Generated by a Sharp Fin at Mach 8.2," AIAA Paper 92-0747, Jan. 1992.

[20]Sun, C. C., and Childs, M. E., "A Modified Wall Wake Velocity Profile for Turbulent Compressible Boundary Layers," *Journal of Aircraft,* Vol. 10, No. 6, 1973, pp. 381–383.

[21]Pulliam, T., and Steger, J., "Implicit Finite-Difference Simulations of Three-Dimensional Compressible Flow," *AIAA Journal,* Vol. 18, No. 2, 1980, pp. 159–167.

[22]Anderson, J. D., *Hypersonic and High Temperature Gas Dynamics,* McGraw Hill, New York, pp. 17–20.

[23]Hopkins, E., Jillie, O., and Sorensen, V., "Charts for Estimating Boundary-Layer Transition on Flat Plates," NASA TN D-5846, June 1970.

[24]Knight, D., "A Hybrid Explicit-Implicit Numerical Algorithm for the Three-Dimensional Compressible Navier-Stokes Equations," *AIAA Journal,* Vol. 22, No. 8, 1984, pp. 1056–1063.

[25]MacCormack, R. W., "A Numerical Method for Solving the Equations of Compressible Viscous Flow," *AIAA Journal,* Vol. 20, No. 9, 1982, pp. 1275–1281.

[26]Narayanswami, N., Horstman, C. C., and Knight, D. D., "Numerical Simulation of Crossing Shock/Turbulent Boundary Layer Interaction at Mach 8.3—Comparison of Zero- and Two-Equation Turbulence Models," AIAA Paper 93-0779, Jan. 1993.

[27]Alvi, F. S., and Settles, G. S., "Structure of Swept Shock Wave/Boundary Layer Interactions Using Conical Shadowgraphy," AIAA Paper 90-1644, June 1990; also, *AIAA Journal,* Vol. 30, No. 9, 1992, pp. 2252–2258.